Chapter 15
Photonic Crystal Fiber as a Lab-in-Fiber Optofluidic Platform

Fei Tian, Svetlana Sukhishvili and Henry Du

Abstract The ability to design and fabricate photonic crystal fiber (PCF) of seemingly unlimited, axially aligned air cladding structures for vastly different optical properties is arguably one of the most significant recent advances in more than half a century of modern fiber optics. The combined characteristics of PCF as both a waveguide for laser transmission/excitation and a microfluidic cell for gas/liquid transport/reactions make it a unique lab-in-fiber platform for chemical and biological processes and their real-time monitoring. The easy access of the fiber air channels for surface functionalization at the molecular and nano scales and the ready incorporation of long-period gratings (LPG) as an integral part of the PCF-based lab-in-fiber platform further expand the realm of its applications. The aim of this chapter is to review the state-of-the-art advances in the science and technology of PCF lab-in-fiber optofluidics relevant to technologically important chemical and biological events and their measurements. The chapter will begin with a brief introduction of the fundamentals, fabrication, optical properties, and general areas of applications of PCF. PCF as a natural lab-in-fiber optofluidics will be highlighted and contrasted with lab-on-chip optofluidics derived from planar silicon device technology. We will then discuss the chemical or biological surface treatment of PCF air channels to impart specific functionality for molecular recognition, the immobilization of plasmonic nanostructures at the channel surface for surface-enhanced Raman scattering and the in situ laser spectroscopy measurements. Considerable focus will be placed on the design, development, and implementation of highly index-sensitive PCF-LPG lab-in-fiber optofluidics for

F. Tian (✉) · S. Sukhishvili · H. Du
Department of Chemical Engineering and Materials Science,
Stevens Institute of Technology, Hoboken, NJ 07030, USA
e-mail: ftian1@stevens.edu

S. Sukhishvili
e-mail: ssukhish@stevens.edu

H. Du
e-mail: hdu@stevens.edu

A. Cusano et al. (eds.), *Lab-on-Fiber Technology*,
Springer Series in Surface Sciences 56, DOI: 10.1007/978-3-319-06998-2_15,

in situ investigation of immunoassays as label-free bioreactors and biosensors as well as for real-time monitoring of layer-by-layer assembly of stimuli-responsive polyelectrolyte thin films as nano-sensors and nano-actuators. We will conclude the chapter by sharing our views on future opportunities and challenges in the exciting field of PCF lab-in-fiber optofluidics.

15.1 Introduction

Silica photonic crystal fiber (PCF, also termed microstructured fiber) represents arguably one of the most exciting recent advances in more than half of a century of fiber optic development [1, 2]. Unlike all-solid conventional optical fiber (COF), which consists typically of high-index core and low-index cladding, the solid- or air-core in PCF is surrounded by a cladding structure composed of a fine array of air channels running axially along the entire fiber length. The diameter of the air channels ranges from sub-microns to tens of microns. The endless degrees of freedom in designing and fabricating the cladding microstructure and thus the ability to realize vastly different and novel optical properties have led to the emergence of PCF as a major field of research. PCF as both a light guide and a microfluidic gas or liquid transmission cell renders it an inherent optofluidic platform, ushering in a promising lab-in-fiber paradigm for a multitude of applications ranging from the monitoring of chemical and biological processes at the molecular level to the study of controlled drug release in technologically and physiologically relevant environment [3].

15.2 PCF as a Light Guide and Its Fabrication

Light is guided in PCF via two mechanisms, depending on fiber microstructure. PCF with a high-index core and a low-index cladding, often found in the solid-core type as illustrated in Fig. 15.1a, operates similarly to that of COF: it guides light by modified total internal reflection, as a result of the index contrast between the solid core and the air-silica cladding. PCF with a low-index core, typically the hollow-type as shown in Fig. 15.1b guides light in the core via the so-called bandgap confinement, made possible by the intricately designed photonic crystal cladding structure [4–7].

Kaiser and Astle [8] reported the first PCF fabrication in 1974. There are two main steps in the fabrication process: the first one always involves preform development that assumes the structure suitable for desired properties; the second one entails fiber drawing at elevated temperature in a drawing tower. Additional steps such as doping can be introduced to meet the need for hybrid fiber types, in

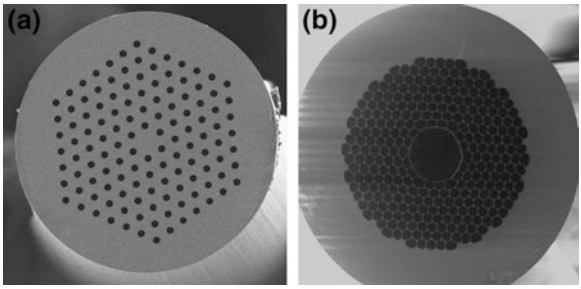

Fig. 15.1 SEM images of **a** *solid-core* PCF with hexagonally arranged cladding air channels and **b** *hollow-core* PCF with photonic bandgap cladding structure

which light guide via both index-guiding and band gap confinement can be accomplished [9].

The preform is often made either by stack and draw method or by sol-gel technique, with the former being the prevailing approach [10]. The stack and draw method has been demonstrated to be versatile to fabricate PCF with complex and diverse cladding microstructures. In this approach, silica capillary tubes and/or rods are directly stacked into a closely packed assembly. The stack is subsequently fused together to form a preform. The preform is drawn to PCF with the desired size and microstructure in a drawing tower. The sol-gel technique is another attractive preform fabrication method because of the significant flexibility in fiber design, its low cost and the ability to produce preforms in large scale [11]. A typical sol-gel casting process developed in OFS Laboratories [12] consists of several steps. First, an array of mandrel elements is arranged in a mold with the designed structure. Then a dispersion of colloidal silica at high pH is filled in the mold. After gelation at lower pH, the mandrel elements are extracted, leaving a series of air channels in the gel body. Thermochemical treatment is employed in the drying and purification processes to help remove undesired water and organic remnants. Finally the gel is sintered at 1,600 °C, resulting in a preform of vitreous glass ready for PCF drawing in the drawing tower.

15.3 PCF as Optofluidics Platform

Microfluidics is the science and technology that manipulates small volumes of fluidic samples in a confined geometry, typically under laminar flow condition [13]. Rapid advance in microfluidics, in conjunction with available micro-fabrication technology, has led to the proliferation of the field of optofluidics [14, 15]. Optofluidics combines microfluidics with propagating light for process control, process monitoring, and sensing and measurements.

The distinct features of PCF optofluidics, compared with its counterpart from planar Si technology, include light path spanning the entire fiber length, low-cost and high-volume fabrication without reliance on photolithography, and easy light coupling. Figure 15.2 shows an example of PCF optofluidics by selectively sealing

the air channels of a hollow-core PCF [16]. This process allows the formation of hybrid PCF with various functional materials filled in the core. UV-curable polymer is infiltrated into the air channels of PCF using a syringe. The flow rate of the polymer is dependent on the dimension of the air channels and the larger hole of fiber core will have a much longer infiltration length. Selective sealing is then achieved by multistep injection-cure-cleave process. Such a hybrid PCF with optical confinement in low index materials is of particular interest for spectroscopy and sensing applications in aqueous solutions. The inherently high rates of mass transport and heat transfer in a microfluidic system make PCF optofluidics an efficient lab-in-fiber micro-reactor with built-in optical interrogation capability for process monitoring.

15.4 PCF as Lab-in-Fiber Microreactor

Photochemistry has been widely used in a variety of applications in photo-medicine [17], chemical synthesis [18], data storage [19] and conversion and storage of solar energy [20]. Monitoring the progress of photochemical reactions in parallel is essential. This capability can be accomplished through miniaturization and integration of sample preparation, optical excitation and detection functionalities, all combined in a single device. These microdevices act as versatile microfluidic platforms which promote the interaction between light and fluids for photochemical activation. There is a surging interest in using PCF for microreactors with nL sample volumes. The intense overlap of the guided light and reactant and product species inside the microchannels of PCF offers exciting new opportunities for in situ spectroscopy of photochemical activation.

The sensitivity and performance of conventional spectroscopic technique using cuvettes is limited by a few centimeters of the interaction path length. This challenge can be overcome using PCF microreactor with path length up to several meters. Moreover, the propagating light is mainly confined in the fiber core, which favors the photochemical activation of the photosensitive compound even with moderate laser power [21]. For example, hollow core PCF has been used as a highly efficient mircoreactor for photolytic conversion of vitamin B12 to vitamin B12b [20] and the photoisomerization of azobenzene derivatives [22].

Platinum-based drugs are well-established anticancer compounds. Traditional drugs do not differentiate cancer cell from healthy tissues, which limits their application due to severe side-effect and acquired resistance. It is of great importance to use photoactivated platinum complexes that can be localized at the tumor site [23]. A highly-controllable photochemical microreactor based on PCF has been demonstrated to simultaneously activate and monitor the reaction dynamics of photoaquation of nontoxic metal complex vitamin B12 (cyanocobalamin, CNCbl) [21]. Figure 15.3 shows the photochemical conversion of CNCbl to $[H_2OCbl]^+$.

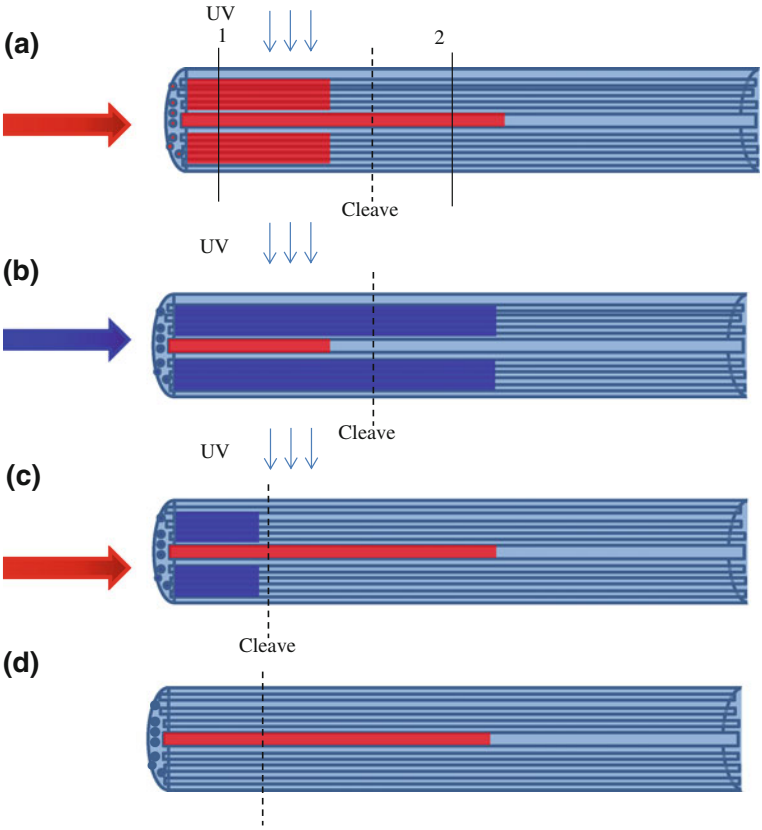

Fig. 15.2 Flow chart of selective filling of the microchannels of PCF. Reproduced with permission [16]

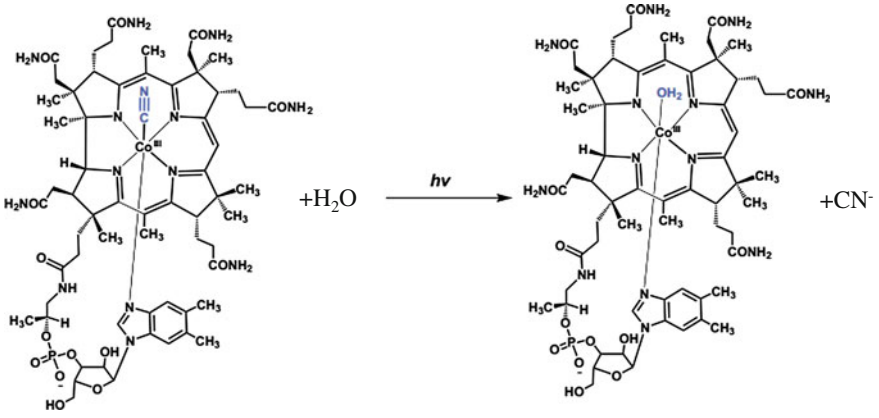

Fig. 15.3 Schematic of photochemical conversion of CNCbl to $[H_2OCbl]^+$ [21]

Because hollow-core PCF allows maximized light-sample interaction inside the hollow core, it is also highly suitable as a spectroscopic nanoreactor for studying and further understanding the catalytic reaction process [24]. For example, it has been employed both as a tubular reactor and a spectroscopic system for studying the well-known photo-Fenton chemistry in which hydrogen peroxide can be decomposed to hydroxyl radicals catalyzed by ferrous ions [24]:

$$Fe^{II} + H_2O_2 \rightarrow Fe^{III} + {}^{\cdot}OH + OH^{-} \tag{15.1}$$

Enhancements in orders of magnitude in both the reaction yield and detection sensitivity can be achieved with PCF, compared with conventional quartz cuvette, due to long path length and efficient overlap with the light field [24].

15.5 PCF as Optofluidic Sensor and Process Monitor

The accessibility to the air channels of PCF has opened up endless possibilities for functionalization of the channel surfaces at the molecular and the nano scales, especially for chem/bio sensing and measurements. Major efforts have been made in this regard such as the incorporation of colloidal nanoparticles, self-assembly multilayers, or nanoporous materials with PCF. Various chemical sensors have been achieved successfully in PCF with such functional coatings in both vapor and aqueous conditions [25]. With the immobilization of bio-specific species, such as specific antigens, complementary strand of DNAs and proteins in PCF, biological sensing and detection can be carried out accordingly. By integrating the fiber with proper indicators or stimuli-responsive materials, a wide range of PCF-based chem/bio sensors can be developed [26, 27]. The review below focuses mainly on two sensing schemes: PCF with built-in surface-enhanced Raman scattering (SERS) functionality for chemical sensing and PCF inscribed with long-period gratings for process monitoring, with the recognition of other applicable sensing modalities such as absorption and fluorescence spectroscopies.

15.5.1 SERS-Active PCF

SERS was discovered in 1974 by Fleischmann et al. who observed intense Raman signal on a roughened silver electrode surface with adsorbed pyridine in aqueous solution [28]. There has been an unabated interest in developing robust SERS substrates for chemical and biological detections ever since. Integrating SERS with PCF takes the advantage of the best of both worlds have to offer for ultra-high sensitivity measurements of minute solutions [29]. With easy access to the cladding air channels for molecular and nano-scale surface modification, a substantial

amount of work has been carried out to impart SERS functionality in PCF with success [30–32].

Gold and silver nanoparticles are extensively used in SERS sensing due to strong surface plasmon resonance when excited by light in the visible to NIR range. There are two strategies to incorporate nanoparticles into PCF. One is to mix the SERS-active nanoparticles with the analyte solution of interest and fill the resultant solution in the cladding air channels of PCF. In one design, gold nanoparticles mixed with Rhodamine B (RhB) aqueous solution was filled in the air channels to about 1 cm long by capillary force [33]. The measurement scheme had a detection limit of 10^{-7} M of RhB, made possible via SERS enhancement. The other strategy, a preferred one, is to immobilize the gold or silver nanoparticles using polyelectrolyte adhesion layer on the air channels of PCF to provide SERS activity along the entire fiber length. A critical step to realize full-length SERS PCF is to ensure the uniformity of immobilized nanoparticles throughout the cladding air channels. Much of our related work has been devoted to achieving this objective with both solid-core and hollow-core PCF for a high-degree of control in the surface coverage density [34–36].

Figure 15.4 shows the cross sectional SEM of solid-core and hollow-core PCF used in this work. A sensitivity of 1×10^{-7} M or $\sim$48 ppb Rhodamine 6G in a minute $\sim 10^{-7}$–10^{-8} L aqueous solution using over 20 cm-long PCF has been demonstrated [34]. Figure 15.5 shows the Raman spectra of 2 μM Rhodamine 6G (R6G) solution using a SERS-active PCF with immobilized silver nanoparticles (1 particle/μm^2) and others as control and reference for the forward propagating geometry [37].

One important criterion in considering PCF for evanescent field-based sensing is the maximization of the mode-field overlap for the light-analyte interaction inside the air channels and the minimization of the confinement loss of the guided modes. By carefully designing the cladding structure of the PCF, the confinement loss decreases and the overlap increases with the increase in the number of rings and diameter of air channels, and the decrease in the web thickness between air channels [38]. For example, we have studied the design of a steering wheel patterned cladding structure of PCF with three large cladding air channels [39]. Numerical simulation of the triangular lattice of the channels demonstrated that confinement loss of less than 0.7 dB/m at 850 nm, and 29, 13.7, and 7.2 % of light intensity overlap in air channels at wavelengths 1,500, 1,000 nm, and 850 nm can be achieved with such a PCF. To assess the effect of cladding microstructure of PCF on the SERS performance of the fiber, three types of PCF have been imparted with SERS functionality and used for SERS measurement of ethanol: nonlinearity PCF (NL PCF) as shown with the core surrounded by six rings of air channels, steering-wheel PCF (SW PCF) and suspended-core PCF (SC PCF) [40]. Numerical analysis showed that the power fractions in the air channels upon filtration with ethanol for the three PCF structures were 0.708, 0.483 and 10.859 %, respectively. Raman measurements were conducted for the three types of PCF with 24 cm in length completely filled with ethanol. The experiments were carried out by laser excitation at one end of the PCF and signal collection at the other end. As shown in

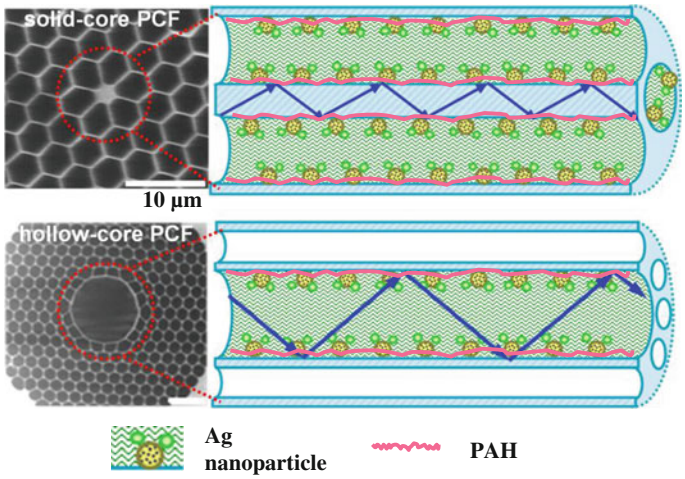

Fig. 15.4 SEM micrographs of *solid-core* PCF and *hollow-core* PCF and schematic illustration of light guiding in the corresponding liquid-filled structures with *Ag nanoparticles* immobilized by positively-charged polyallylamine hydrochloride (*PAH*). Reproduced with permission [34]

Fig. 15.6, the ratio of Raman intensities at 2,930 cm^{-1} (characteristic of C–H stretching vibration from ethanol) for SW PCF, NL PCF, and SC PCF was about ~1:14:28, in qualitative agreement with the numerical results.

Different from solid-core PCF, hollow-core PCF provides a sensing platform for direct interaction between light and analyte present in the hollow core. We have demonstrated a full-length liquid-core PCF with the fiber length up to 30 cm for SERS detection in a forward propagating mode [34]. The key to achieving the full-length liquid-core PCF for SERS detection is to incorporate a uniform layer of SERS-active nanoparticles inside the hollow core along the entire length of the PCF with relatively low surface coverage density. Figure 15.7a shows the Raman spectrum obtained for hollow-core PCF with the core filled with 10^{-5} M R6G. Figure 15.7b, c and d show three hyperspectral Raman images corresponding to silica (485 cm^{-1}), R6G (1,351 cm^{-1}), and water (3,381 cm^{-1}) in liquid-core PCF. The dashed ring-like Raman distribution in Fig. 15.7b indicates that the core and two adjacent air channels allowed forward propagating of silica signal. Core mode contribution to the measured Raman intensities can also be demonstrated by the confinement of the Raman distributions for R6G and water as shown in Fig. 15.7c and d. The above results strongly suggested that the hollow-core PCF can be suitable as a highly sensitive SERS-active platform due to the robust waveguide upon infiltration with liquid, the effective coupling of R6G to SERS signal and forward-propagation of the Raman signal along the liquid core.

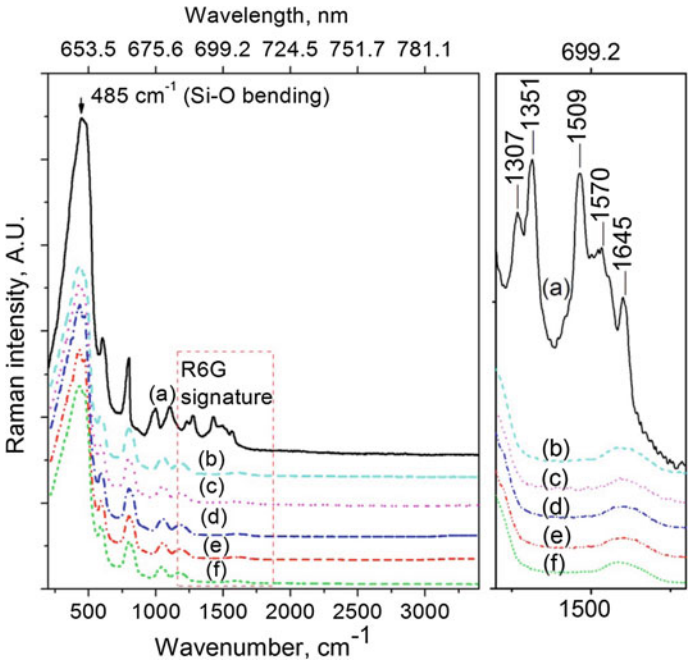

Fig. 15.5 Raman spectra for *a* SERS-active PCF filled with 2 μM R6G solution, *b* SERS-active PCF filled with water, *c* PCF with adsorbed gelatin and filled with R6G solution, *d* PCF with adsorbed gelatin and filled with water, *e* PCF filled with water, and *f* bare PCF. The right panel corresponds to spectral enlargement in the region of characteristic peaks of R6G. The forward Raman measurements were done at 632.8 nm, ∼5 mW laser power, and acquisition time of 10 s. Reproduced with permission [37]

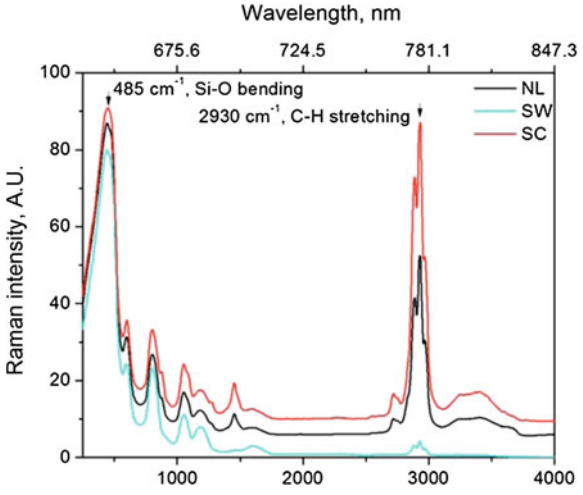

Fig. 15.6 Raman spectra from NL PCF, SW PCF, and SC PCF filled with ethanol. The Raman measurements were carried out at 632.8 nm and 5 mW power, with an acquisition time of 20 s. Reproduced with permission [40]

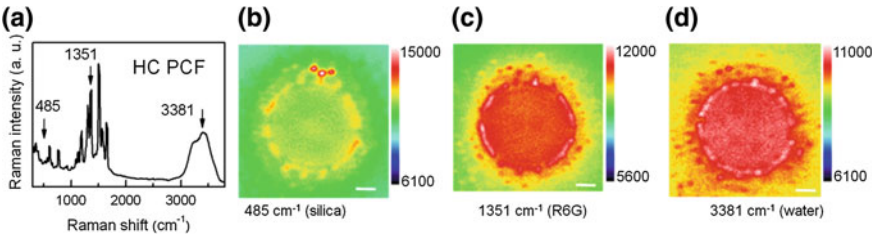

Fig. 15.7 SERS spectra of 10^{-5} M R6G (**a**) and hyperspectral Raman images of silica (**b**), R6G (**c**), and water (**d**) from hollow-core PCF with immobilized silver nanoparticles of ~0.5 particle/μm2 in coverage density. The measurements were done using forward-propagating geometry at an excitation wavelength of 632.8 nm. Reproduced with permission [34]

15.5.2 Long-Period Gratings in PCF as Index Transduction Platform

Long-period gratings (LPG) in PCF are periodical modulations of the refractive index axially along the fiber with a period in the range of 100 μm to 1 mm. The core mode of LPG is coupled to the forward propagating cladding mode at some resonance wavelength, resulting in significant attenuation in its transmission spectrum. The resonance wavelength, λ, is described by phase matching condition $\lambda = (n_{core}^{eff} - n_{clad}^{eff})\wedge$, where, $(n_{core}^{eff}$ and $(n_{clad}^{eff}$ are respective effective indices of the core and the cladding modes, and Λ is grating period. The strong dependence of λ on $(n_{clad}^{eff}$ makes LPG in PCF an optofluidic platform that is highly sensitive to the changes in $(n_{clad}^{eff}$ induced by any physical, chemical, or biological perturbations in the cladding structure. The ability to bring a measurant solution inside of the cladding air channels to directly interact with the cladding mode further boosts the refractive index sensitivity of PCF-LPG.

Periodic index perturbation in LPG can be accomplished by laser techniques such as UV, infrared femtosecond laser or CO_2 laser irradiation as well as by non-laser approaches such as arc discharge, acoustic wave coupling, focused ion beam and periodic mechanical stress loading. CO_2 laser irradiation is advantageous due to system flexibility and ease of control. While silica material itself has a very low absorption at the wavelength of UV light, CO_2 laser is readily utilized as a versatile tool for LPG fabrication in PCF due to the strong absorption of the silica material at the wavelength of 10.6 μm. Many studies have focused on the investigation of the LPG coupling mechanism associated with CO_2 laser for various types of fibers [41, 42]. LPG fabricated by CO_2 laser exhibits good temperature stability [43].

15.5.2.1 PCF-LPG as Optofluidic Platform for Sensing in Liquid Phase

Refractive index is a fundamental material property that is of great importance in science and technology. The detection of minute deviations in refractive index is essential for process control and quality assurance in pharmaceutical, beverage and food industries, for instance. There is a growing interest in the development of PCF-LPG for such applications. The sensitivity of PCF-LPG increases significantly with the refractive index of the probing medium. This correlation makes PCF-LPG especially suited for liquid phase measurements.

PCF-LPG has been shown to be sensitive to adsorption of nanometer thick biomolecules such as DNA and proteins [44]. The performance of PCF-LPG based biosensor has been further enhanced by integrating it with a flow cell [45]. The microfluidic cell can optically couple light into and out of PCF while enabling continuous liquid flow through the air channels as part of an integral surface modification/binding and *in situ* measurement scheme [45]. The negatively charged inner surface of the microchannels in the PCF is modified by electrostatic self-assembled polymer monolayer for the subsequent adsorption of antibody. Upon exposure of the modified surface to specific secondary antibody, there is a resonance wavelength shift due to the adsorption of the specific secondary antibody. The PCF-LPG can thus monitor each and every step of the multiple modification and binding sequences. This optofluidics device scheme has been shown to be sensitive to monolayer adsorption/binding event [45].

15.5.2.2 PCF-LPG as Optofluidic Platform for Layer-by-Layer Process Monitoring

Layer-by-layer (LbL) assembly, first introduced by Decher in 1997 [46], has been regarded as a robust processing method to obtain thin films with multi-functionalities. The LbL technique has been used to produce ultrathin films at interface by sequential alternating adsorption of polymers from solutions. The technique has received growing attention as a simple and environmentally benign way to create advanced surface coatings with a nanoscopically controlled structure. LbL approach is advantageous in several ways. First, it is able to incorporate with a wide range of functional molecules, such as electroactive polymers, organic dyes, semiconductor quantum dots, electrochemically active species, inorganic nanomaterials, and biologically active molecules within nanostuctured films (see Fig. 15.8) [47–49]; Second, LbL layers can be functionally designed to respond to environmental stimuli such as pH, ionic strength, temperature, and light irradiation, imparting distinct physical, chemical, and biological properties in the films and/or coated surface itself; Third, it can be deposited virtually on the surface of substrate with any shape and chemistry.

Integrating LbL assembly in the air channels of the PCF-LPG of high index sensitivity thus create another exciting opportunity to monitor and understand the LbL process in microfluidic systems and to develop similarly configured

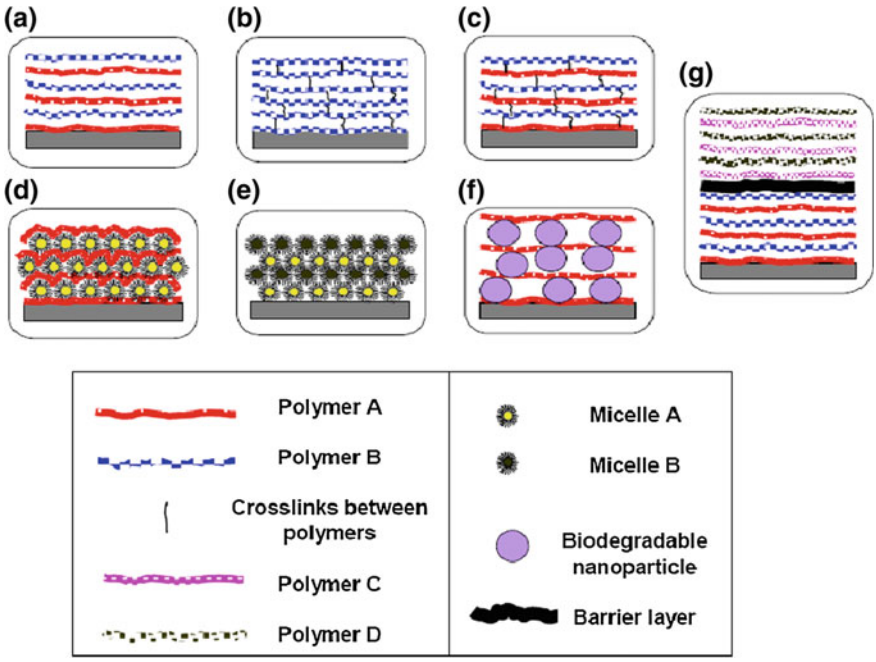

Fig. 15.8 Schematic illustration of various nanostructured materials prepared via LbL. The depicted structures represent: **a** a polymer/polymer non-crosslinked LbL film, **b** a single-component crosslinked hydrogel, **c** a two-component crosslinked hydrogel, **d** a polymer/micelle coating, **e** a micelle/micelle coating, **f** a polymer/biodegradable nanoparticle film, and **g** a stratified film with a barrier layer in between. Reproduced with permission [47]

microsensors and microactuators. Shown in Fig. 15.9 is an optically coupled flow chamber that we have used to perform real-time and in situ transmission measurements during LPG fabrication and LbL assembly under continuous flow of the liquid medium through the PCF air channels [50].

The LbL procedure basically involves the immersing of the platform surface in alternating polyelectrolyte solutions, between which thorough rinsing is employed to remove excess polymer molecules. The specific steps for LbL in PCF-LPG are depicted in Fig. 15.10.

In one set of experiments, the PCF-LPG (1.37 cm in length and 490 μm in periodicity) was precleaned with 10 wt% hydrogen peroxide and Millipore (Milli-Q system) filtered water. One bilayer of BPEI/PMAA was deposited and thermally cross-linked at 125 °C for 1 h for enhanced adhesion. PVPON/PMAA multilayers were deposited from 0.2 mg/ml polymer solution at pH 2. Each step was followed by rinsing with 0.01 M phosphate buffer solution at the same pH. After six bilayers of PVPON/PMAA were deposited in the PCF-LPG, the PMAA layers were chemically cross-linked including activation in EDC solution (5 mg/ml, pH = 5) and subsequent treatment in AADH cross-linker solution (9 mg/ml, pH = 4). PVPON

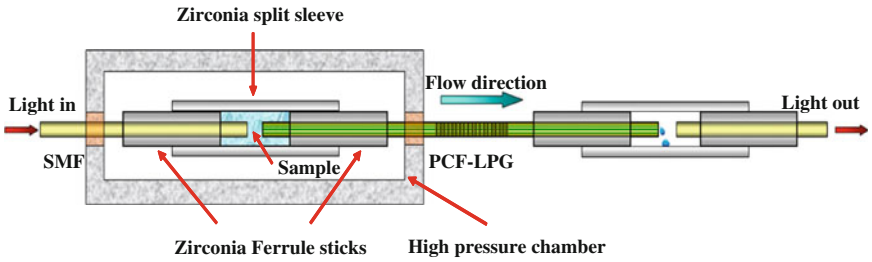

Fig. 15.9 Optically coupled microfluidic module for LbL in PCF-LPG and in situ transmission measurements. Reproduced with permission [50]

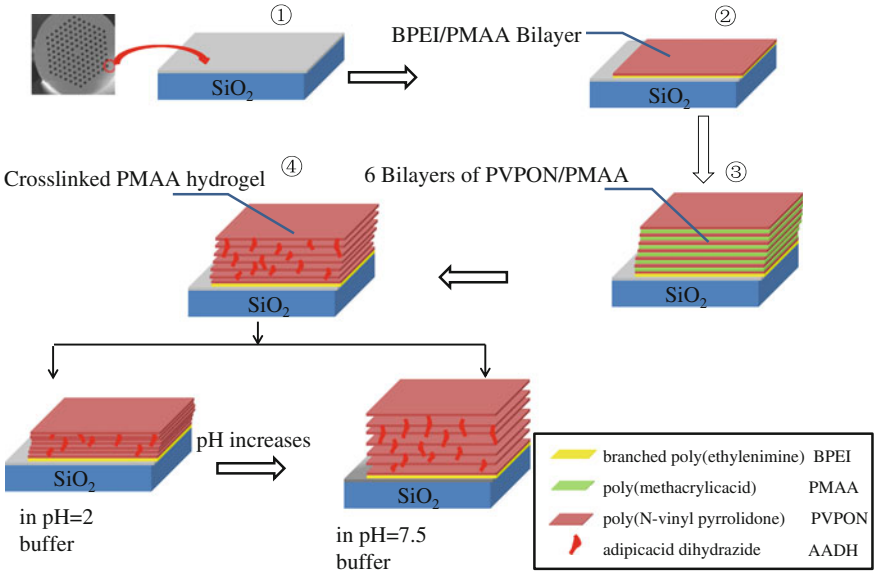

Fig. 15.10 Schematic of the procedures of LbL deposition of PVPON/PMAA and formation of PMAA hydrogel in PCF-LPG with BPEI/PMAA as adhesion bilayer. Reproduced with permission [50]

molecules were removed from the thin film by exposure to 0.01 M phosphate buffer solution with pH 7.5. The same procedures were performed using COF-LPG (2.49 cm in length and 710 μm in periodicity) in another set for comparison. Fluorescently labeled PMAA was used for the deposition in the last layer in order to examine the distribution of the thin film that's fabricated on the fiber under confocal microscopy. Shown in Fig. 15.11 is the confocal microscopy of the PMAA hydrogel on COF and in PCF, confirming that a PMAA hydrogel has been successfully deposited using both LPG platforms.

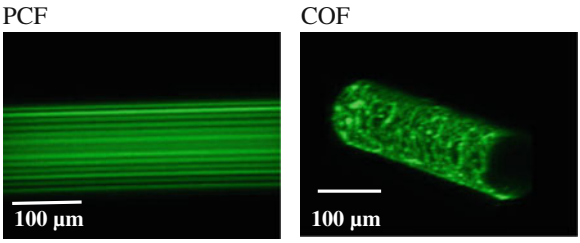

Fig. 15.11 Confocal microscopy of the PMAA hydrogel on *COF* and in *PCF*

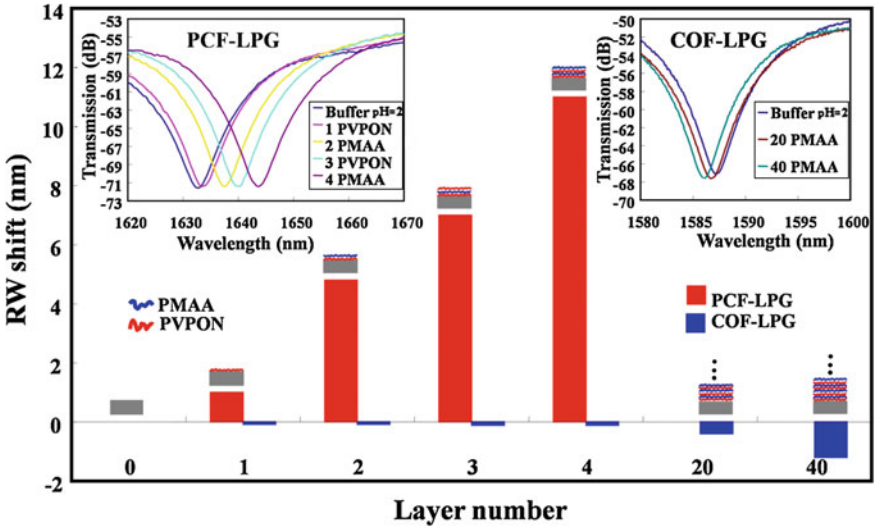

Fig. 15.12 Respective RW shifts in response to LbL assembly of PVPON and PMMA in PCF-LPG and on COF-LPG. Insets are the corresponding transmission spectra. reproduced with permission [50]

An optical spectrum analyzer was used to measure the transmission spectrum at each LbL step followed by buffer rinsing. The RW for PCF-LPG with buffer at approximately 1,678 nm arises from core mode to LP_{04} cladding mode coupling according to our numerical calculations and was used in our analysis. The RW of the PCF-LPG underwent a dramatic red shift (to longer wavelength) as the PVPON/PMAA LbL assembly was successively carried out in the cladding air channels. In contrast, a slight blue shift (to short wavelength) in RW took place for LbL processes on COF-LPG. Summarized in Fig. 15.12 are the respective shifts in RW as PVPON and PMAA layers were alternately deposited in PCF-LPG and on COF-LPG.

The red bars denote red shift in PCF-LPG and blue bars represent blue shift in COF-LPG. Six LbL bilayers in PCF-LPG produced a shift of $\sim$19.5 nm in RW (equivalent to $\sim$1.625 nm shift per LbL layer). In contrast, 20 LbL bilayers on

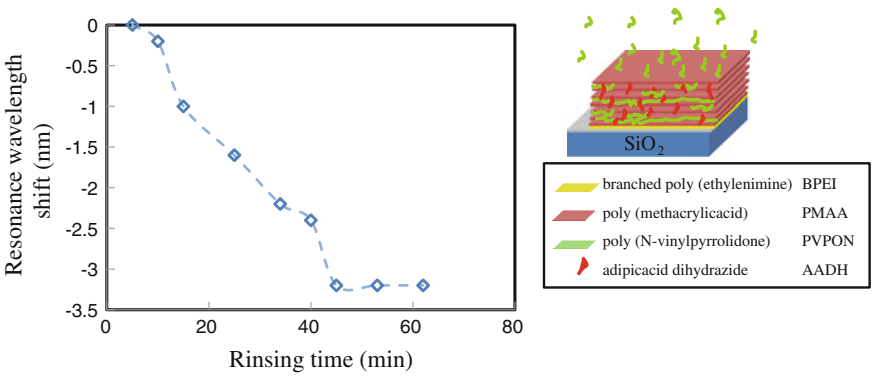

Fig. 15.13 Schematic of PVPON release from LbL film and time-dependent shift in RW as the process takes place in PCF-LPG. Reproduced with permission [50]

COF-LPG yielded only a shift of ~1 nm total (equivalent to ~0.025 nm/layer). The opposite direction in RW shift for PCF-LPG and COF-LPG accompanied with LbL deposition is a result of their drastically different dispersion characteristics of effective refractive indices of the cladding modes [51]. The ~65 fold increase in the sensitivity of PCF-LPG over COF-LPG can be attributed to higher evanescent field overlap with cladding air channels that also provide a far larger surface area for LbL growth. In contrast, COF-LPG only probes the LbL films on the outer surface of the all-solid fiber. The high sensitivity of PCF-LPG also enabled in situ monitoring of PVPON release from cross-linked PMAA layers in phosphate buffer at pH 7.5. Figure 15.13 shows blue shift in RW as PVPON was gradually released from the LbL film in PCF-LPG. The blue shift is expected per phase matching condition since the removal of PVPON results in a reduction in the effective index of refraction in the thin film. The stable RW after ~45 min suggests completion of the release process. Total release of PVPON transformed the LbL film to a pH-responsive PMAA hydrogel. This process afforded us the opportunity to test hydrogel-containing PCF-LPG as well as COF-LPG as potential pH sensors. Specifically, the RW shifts of the two systems were measured by exposing them to phosphate buffers (pH: 2–7.5). The pH-dependent transmission and RW shift are illustrated in Fig. 15.14.

There is a pronounced increase in the RW of the PCF-LPG (red bars) with decreasing pH, indicating higher refractive index of the thin film. In contrast, the RW shift for COF-PCF (blue bars) in response to pH variation is far less robust. It is well known that PMAA hydrogel tends to be increasingly deprotonated at higher pH, leading to stronger repulsion between the ionized carboxylic groups and swelling of the hydrogel. Increased swelling corresponds to decreased index of refraction of the hydrogel. The opposite shift in RW and the striking difference in sensitivity between PCF-LPG and COF-LPG can be similarly explained as for the results in Fig. 15.12. pH response behavior of the PMAA hydrogel is interpreted by the conformational change of PMAA as illustrated by Fig. 15.15.

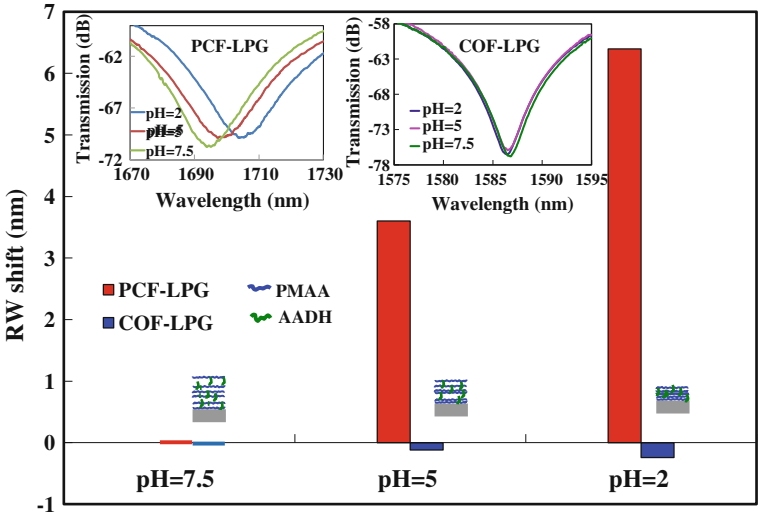

Fig. 15.14 pH-dependent transmission and RW shift for PCF-LPG and COF-LPG coated with PMAA hydrogels. Reproduced with permission [50]

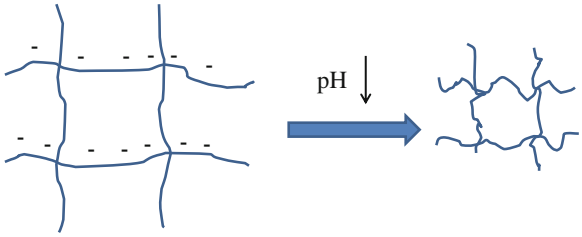

Fig. 15.15 Conformational change of PMAA thin film in buffer solution with different pH

The pH responsiveness of PMAA hydrogel has been demonstrated on flat geometry in [52]. The PMAA surface-attached hydrogels are highly swollen in water, and their swelling degree can be controlled between 1.2 and 3 by varying the degree of film crosslinking [52]. Most importantly, the swelling degree of these films is strongly pH dependent (Fig. 15.16).

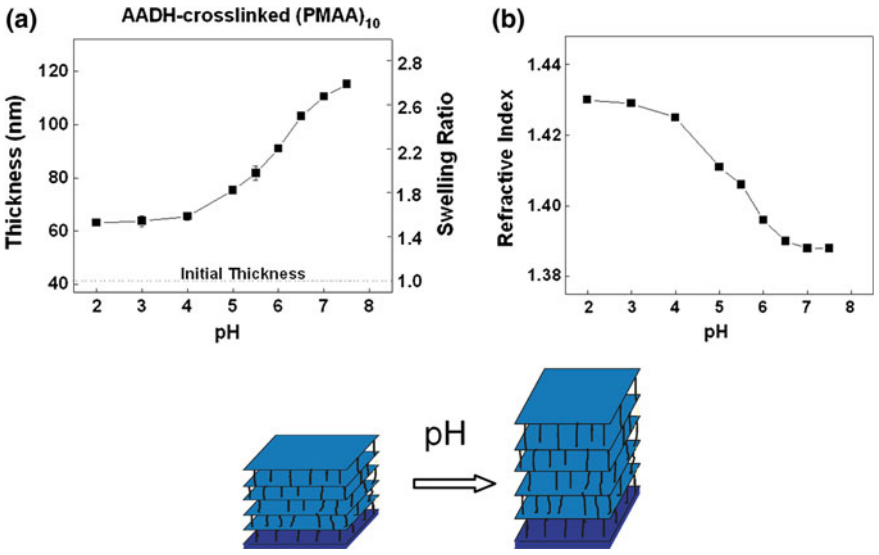

Fig. 15.16 Panels (**a**) and (**b**): swelling ratios and refractive indices of $(PMAA)_{10}$ films crosslinked with adipic acid dihydrozide (AADH) as a function of pH supported by 0.01 M phosphate buffer by in situ ellipsometry. The thickness of the dry $(PMAA)_{10}$ films was $\sim$41 nm. Reproduced with permission [52]

15.6 Concluding Remarks

The ability to design, fabricate, and functionalize PCF of seemingly unlimited microstructural features for vastly different optical characteristics affords us endless opportunities for research creativity and innovation. PCF as an inherent optofluidic platform allows the exploration and harvesting of intimate light-medium interactions in the air channels of ultra-large aspect ratio for chemical and biological synthesis, for process control, and for the development of novel sensing devices, all with real-time and in-situ capabilities. Significant progress has been made by the scientific community in advancing the frontier of PCF for related applications. PCF research in the context of lab-in-fiber optofluidics is still at its infancy. This field of research will undoubtedly undergo exponential growth in the coming decade, leading to new science, technology, and yet-to-be-foreseen applications.

Acknowledgments This chapter contains a significant amount of our prior and ongoing studies funded by the US National Science Foundation under grants ECCS-0404002, ECCS-0922175 and DMR-0906474. We thank the various colleagues of ours for their contributions to the work reviewed.

References

1. J.C. Knight, Photonic crystal fibres. Nature **424**, 847–851 (2003)
2. P.St.J. Russell, Photonic crystal fibers. Science **299**, 358–362 (2003)
3. J.C. Knight, T.A. Birks, P.S.J. *Russell, in Optics of Nanostructured Materials*, eds. by V.A. Markel, T.F. George (Wiley, New York, 2001), pp. 39–71
4. T.A. Birks, P.J. Roberts, P.J. Russell, D.M. Atkin, T.J. Shepherd, Full 2-D photonic bandgaps in silica/air structures. Electron. Lett. **31**, 1941–1943 (1995)
5. J.C. Knight, J. Broeng, T.A. Birks, P.J. Russell, Photonic band gap guidance in optical fibers. Science **282**, 1476–1478 (1998)
6. R.F. Cregan, B.J. Mangan, J.C. Knight, T.A. Birks, P.J. Russell, P.J. Roberts, D.C. Allan, Single-mode photonic band gap guidance of light in air. Science **285**, 1537–1539 (1999)
7. J.C. Knight, P.J. Russell, New ways to guide light. Science **296**, 276–277 (2002)
8. P.V. Kaiser, H.W. Astle, Low-loss single-material fibers made from pure fused silica. Bell Syst. Tech. J. **53**, 1021–1039 (1974)
9. A. Cerqueira S.Jr., F. Luan, C.M.B. Cordeiro, A.K. George, J.C. Knight, Hybrid photonic crystal fiber, Opt. Express **14**, 926–931 (2006)
10. J.C. Knight, T.A. Birks, P.J. Russell, D.M. Atkin, All-silica single-mode optical fiber with photonic crystal cladding. Opt. Lett. **21**, 1547–1549 (1996)
11. R. Bise, D.J. Trevor, Solgel-derived mircrostructured fibers: fabrication and characterization, in *Conference on Optical Fiber Communication, Technical Digest Series*, Anaheim, CA, vol. 3 pp. 269–271 (2005)
12. R. Bise, Manufacturing of microstructured optical fibers (2006). http://www.cns.cornell.edu/documents/RyanBiseOFSLaboratories.pdf
13. G.M. Whitesides, The origins and the future of microfluidics. Nature **442**, 368–373 (2006)
14. H.A. Stone, A.D. Stroock, A. Ajdari, Engineering flows in small devices: microfluidics toward a lab-on-a-chip. Ann. Rev. Fluid Mech. **36**, 381–411 (2004)
15. J. Hecht, *City of Light: The Story of Fiber Optics* (Oxford University Press, New York, 1999)
16. Y.Y. Huang, Y. Xu, A. Yariv, Fabrication of functional microstructured optical fibers through a selective-filling technique. Appl. Phys. Lett. **85**, 5182–5184 (2004)
17. Z. Huang, A review of progress in clinical photodynamic therapy. Technol. Cancer Res. Treat. **4**, 283–293 (2005)
18. N. Homann, Photochemical reactions as key steps in organic synthesis. Chem. Rev. **108**, 1052–1103 (2008)
19. F. Li, J. Zhuang, G. Jiang, H. Tang, A. Xia, L. Jaing, Y. Song, Y. Li, D. Zhu, A rewritable optical data storage material system by [2 + 2] photocycloreversion—photocycloaddition. Chem. Mater. **20**, 1194 (2008)
20. M. Grätzel, Solar energy conversion by dye-sensitized photovoltaic cells. Inorg. Chem. **44**, 6841–6851 (2005)
21. J.S.Y. Chen, T.G. Euser, N.J. Farrer, P.J. Sadler, M. Scharrer, P.J. Russell, Photochemistry in photonic crystal fiber nanoreactors. Chem.—Eur. J. **16**, 5607–5612 (2010)
22. J.S.Y. Chen, T.G. Euser, G.O. Williams, A.C. Jones, P.S.T. Russell, Photoswitching in Photonic Crystal Fiber, in *Conference on Optical Sensors, Karlsruhe Germany*, (Optical Society of America, 2010), paper SThB4
23. W.M. Sharman, C.M. Allen, J.E. van Lier, Photodynamic therapeutics: basic principles and clinical applications. Drug Discov. Today **4**, 507–517 (1999)
24. A.M. Cubillas, M. Schmidt, M. Scharrer, T.G. Euser, B.J.M. Etzold, N. Taccardi, P. Wasserscheid, P.S.J. Russell, Ultra-low concentration monitoring of catalytic reactions in photonic crystal fiber. Chem.—Eur. J. **18**, 1586–1590 (2012)
25. V.P. Minkovich, D. Monzon-Hernandez, J. Villatoro, G. Badenes, Microstructured optical fiber coated with thin films for gas and chemical sensing. Opt. Express **14**, 8413–8418 (2006)
26. M. Skorobogatiy, Microstructured and photonic bandgap fibers for applications in the resonant bio- and chemical sensors. J. Sens. **2009**, 524237 (2009)

27. T.M. Monro, S. Warren-Smith, E.P. Schartner et al., Sensing with suspended-core optical fibers. Opt. Fiber Technol. **16**, 343–356 (2010)
28. M. Fleischmann, P.J. Hendra, A.J. McQuillan, Raman spectra of pyridine adsorbed at a silver electrode. Chem. Phys. Lett. **26**, 163–166 (1974)
29. H. Yan, C. Gu, C. Yang, J. Liu, G. Jin, J. Zhang, L. Hou, Y. Yao, Hollow core photonic crystal fiber surface-enhanced Raman probe, Appl. Phys. Lett. **89**, Article ID 204101, (2006)
30. Y. Zhang, C. Shi; C. Gu, L. Seballos, J.Z. Zhang, Liquid core photonic crystal fiber sensor based on surface enhanced Raman scattering, Appl. Phys. Lett. **90**, Article ID 193504 (2007)
31. F.M. Cox, A. Argyros, M.C.J. Large, S. Kalluri, Surface enhanced Raman scattering in a hollow core microstructured optical fiber. Opt. Express **15**, 13675–13681 (2007)
32. A. Amezcua-Correa, J. Yang, C.E. Finlayson, A.C. Peacock, J.R. Hayes, P.J.A. Sazio, J.J. Baumberg, S.M. Howdle, Surface-enhanced Raman scattering using microstructured optical fiber substrates. Adv. Funct. Mater. **17**, 2024–2030 (2007)
33. Yan, J. Liu, C. Yang, G. Jin, C. Gu, and L. Hou, Novel index-guided photonic crystal fiber surface-enhanced Raman scattering probe, Opt. Express **16**, 8300–8305 (2008)
34. Y. Han, S. Tan, M.K. Khaing Oo, D. Pristinski, S. Sukhishvili, H. Du, Towards full-length accumulative surface-enhanced raman scattering-active photonic crystal fibers. Adv. Mater. **22**, 2647–2651 (2010)
35. R.G. Freeman, K.C. Grabar, K.J. Allison, R.M. Bright, J.A. Davis, A.P. Guthrie, M.B. Hommer, M.A. Jackson, P.C. Smith, D.G. Walter, M.J. Natan, Self-assembled metal colloid monolayers: an approach to SERS substrates. Science **267**, 1629–1632 (1995)
36. M. Erol, Y. Han, S.K. Stanley, C.M. Stafford, H. Du, S. Sukhishvili, SERS not to be taken for granted in the presence of oxygen. J. Am. Chem. Soc. **131**, 7480–7481 (2009)
37. M.K. Khaing Oo, Y. Han, R. Martini, S. Sukhishvili, H. Du, Forward-propagating surface-enhanced Raman scattering and intensity distribution in photonic crystal fiber with immobilized Ag nanoparticles, Opt. Lett. **34**, 968–970 (2009)
38. T.P. White, R.C. McPhedran, C.M. De Sterke, L.C. Botten, M.J. Steel, Confinement losses in microstructured optical fibers. Opt. Lett. **26**, 1660–1662 (2001)
39. Y. Zhu, H. Du, R. Bise, Design of solid-core microstructured optical fiber with steering-wheel air cladding for optimal evanescent-field sensing. Opt. Express **14**, 3541–3546 (2006)
40. M.K. Khaing Oo, Y. Han, J. Kanka, S. Sukhishvili, H. Du, Structure fits the purpose: Photonic crystal fibers for evanescent-field surface-enhanced Raman spectroscopy, Opt. Lett. **35**, 466–468 (2010)
41. H.W. Lee, Y. Liu, K.S. Chiang, Writing of long-period gratings in conventional and photonic-crystal polarization-maintaining fibers by CO_2-laser pulses. IEEE Photon. Technol. Lett. **20**, 132–134 (2008)
42. B.H. Kim, Y. Park, T.J. Ahn, B.H. Lee, Y. Chung, U.C. Paek, W.T. Han, Residual stress relaxation in the core of optical fiber by CO_2 laser radiation. Opt. Lett. **26**, 1657–1659 (2001)
43. D.D. Davis, T.K. Gaylord, E.N. Glytsis, S.C. Mettler, Very-high-temperature stable CO2 laser-induced longperiod fibre gratings. Electron. Lett. **35**, 740–742 (1999)
44. L. Rindorf, J.B. Jensen, M. Dufva, L.H. Pedersen, P.E. Høiby, O. Bang, Photonic crystal fiber long-period gratings for biochemical sensing. Opt. Express **14**, 8224–8231 (2006)
45. Z. He, F. Tian, Y. Zhu, N. Lavlinskaia, H. Du, Long-period gratings in photonic crystal fiber as an optofluidic label-free biosensor. Biosens. Bioelectron. **26**, 4774–4778 (2011)
46. G. Decher, Fuzzy nanoassemblies: toward layered polymeric multicomposites. Science **277**, 1232–1237 (1997)
47. S. Pavlukhina, S. Sukhishvili, Polymer assemblies for controlled delivery of bioactive molecules from surfaces. Adv. Drug Deliver. Rev. **63**, 822–836 (2011)
48. E. Kharlampieva, V. Kozlovskaya, S.A. Sukhishvili, Layer-by-layer hydrogen-bonded polymer films: from fundamentals to applications. Adv. Mater. **21**, 3053–3065 (2009)
49. Z. Tang, Y. Wang, P. Podsiadlo, N.A. Kotov, Biomedical applications of layer-by-layer assembly: from biomimetics to tissue engineering. Adv. Mater. **18**, 3203–3224 (2006)
50. F. Tian, J. Kanka, S. Sukhishvili, H. Du, Photonic crystal fiber for layer-by-layer assembly and measurements of polyelectrolyte thin films. Opt. Lett. **37**, 4299–4301 (2012)

51. Y. Zhu, Z. He, J. Kanka, H. Du, Numerical analysis of refractive index sensitivity of long-period gratings in photonic crystal fiber. Sens. Actuators, B **129**, 99–105 (2008)
52. S. Pavlukhina, Y. Lu, A. Patimetha, M. Libera, S. Sukhishvili, Polymer multilayers with pH-triggered release of antibacterial agents. Biomacromolecules **11**, 3448 (2010)